



Published in final edited form as:

*Lab Chip*. ; 22(11): 2145–2154. doi:10.1039/d2lc00162d.

## Cellular point-of-care diagnostic using an inexpensive layer-stack microfluidic device

Kilean Lucas<sup>1</sup>,

Juhyun Oh<sup>1</sup>,

Jan Hoelzl<sup>1,3</sup>,

Ralph Weissleder<sup>1,2,\*</sup>

<sup>1</sup>Center for Systems Biology, Massachusetts General Hospital, 185 Cambridge St, CPZN 5206, Boston, MA 02114,

<sup>2</sup>Department of Systems Biology, Harvard Medical School, 200 Longwood Ave, Boston, MA 02115

<sup>3</sup>Medical Oncology, Heidelberg University Medical Center, Heidelberg, Germany

### Abstract

Cellular analyses are increasingly used to diagnose diseases at point-of-care and global healthcare settings. Some analyses are simple as they rely on chromogenic stains (blood counts, malaria) but others often require higher multiplexing to define and quantitate cell populations (cancer diagnosis, immunoprofiling). Simplifying the latter with inexpensive solutions represents a current bottleneck in designing start-end pipelines. Based on the hypothesis that novel film adhesives could be used to create inexpensive disposable devices, we tested a number of different designs and materials, to rapidly perform 12–15 channel single-cell imaging. Using an optimized passive pumping layer-stack microfluidic (PLASMIC) device (< 1\$ in supplies) we show that rapid, inexpensive cellular analysis is feasible.

### Keywords

point-of-care; diagnostic; single cell analysis

---

\*R. Weissleder, MD, PhD, Center for Systems Biology, Massachusetts General Hospital, 185 Cambridge St, CPZN 5206, Boston, MA, 02114, 617-726-8226, rweissleder@mgh.harvard.edu.

Contributions

Design: KL, RW

Experiments: KL, JO

Data analysis and figures: all authors

Writing: RW, KL, JO

Conflict of interest

RW is a consultant to ModeRNA, Tarveda, Lumicell, Seer, Earli, Alivio Therapeutics, Aikili Biosystems and Accure Health. Other authors report no industrial interactions.

## Introduction

Appropriate cancer treatments increasingly rely on the molecular analysis of harvested cells or tissue. Tumor tissue is often sampled by surgical excisional/incisional biopsy, image-guided core biopsy, or fine needle aspiration biopsy (FNA), yielding different amounts of tissue for subsequent analysis. While all three methods are commonly used in advanced healthcare systems, there has been an interest in obtaining deeper and more complete data with less invasive procedures such as FNA. For example, COVID-19 has placed unprecedented strain on access to cancer care, highlighting the need for rapid, decentralized diagnostics that reduce the need for invasive and complex inpatient procedures. Another major application is for uncomplicated diagnostics in low and middle income countries where access to sophisticated technology or expert analyses is lacking. In these settings, FNA procedures can be ideal as they have lower complication rates than core biopsies and are generally very well-tolerated due to the use of smaller gauge needles (20–27 G)<sup>1, 2</sup>. Recent research has focused on developing automated pipelines for comprehensive analysis of FNA tumor samples. This has included development of cyclic staining methods for high multiplexing<sup>3, 4</sup>, automated imaging systems<sup>5</sup> and AI-enabled software<sup>6</sup>. One missing piece to the puzzle, however, has been the development of robust sample handling methods for cell immobilization and repeat staining cycles.

Microfluidic devices are highly customizable platforms that allow for a variety of applications while minimizing sample consumption<sup>7, 8</sup>. Overall, this reduces the cost of reagents by using less overall volume, providing a more affordable platform for single-cell analysis. While highly complex microfluidic devices can be manufactured to perform a multitude of operations and can incorporate features such as valves, pumps and filters, the traditional approach to the fabrication of these devices is generally complex, costly and error-prone. As a result, simpler solutions are required, especially for low and middle income countries (LMIC) and other point-of-care environments. Several such devices and applications have been reported<sup>9–14</sup> but many of them remain complex and require specialized manufacturing equipment. For example, simple PDMS flow channels require technical/expensive manufacturing environments to reduce dust contamination in the device. While improvements have been made in reducing the cost of the equipment needed for manufacturing molds, these are also expensive instruments (~\$6,000<sup>15</sup>) that a clinician would need the training to operate. Other simple microfluidic systems that use capillary action to drive flow are typically paper-based devices that are not viable for imaging cell samples<sup>16</sup>.

We reasoned that a simple and inexpensive device could be created by using acrylic pressure sensitive adhesives (PSA) to bond coverslips to a microscopic slide in such a fashion that liquid movement (staining, de-staining, washing) could be performed on chip without the need for an active pump. Indeed, we found that cheap and effective passive pumping layer-stack microfluidics (PLASMIC) can be assembled without the need for special tools. To exchange fluids in PLASMIC devices, the properties of surface tension are exploited using passive pumping. By forming droplets of differing sizes on the inlet and outlet of the devices, it is possible to generate sufficient flow in place of an electric pump. In this work, we describe the development, testing, validation, and scale-up of such microfluidic

devices for the cyclic imaging of immune and tumor markers. This described device allows for reduced reagent consumption and improved imaging reliability. Furthermore, using a desktop craft cutter to produce the PLASMIC device is a low-cost, user-friendly method available to clinicians and non-scientists alike. The simple and inexpensive device will make single-cell cyclic imaging more accessible to a broad scientific/medical community. Notably, the described device has potential for global diagnostics in remote and resource-limited biomedical environments<sup>5</sup>.

## Results

### Design criteria

The proposed passive pumping layer-stack microfluidic (PLASMIC) approach to performing immune and tumor phenotyping is composed of 4 major steps (Figure 1A). First, a cellular sample is collected via fine needle aspirate (FNA) or cell culture. The suspension is fixed in the PLASMIC device and cyclic imaging is performed by presenting antibodies for immune or tumor markers. These antibodies are quenched after each cycle of 3 markers to free up the channels for the next round of labeling. The data is then processed for cell type classification and phenotyping that can provide diagnostic/prognostic information about the sample.

A render of the PLASMIC device used for these experiments is shown in Figure 1A, where the two layers of the system are revealed. A poly-L-lysine slide is used as the base substrate to which cells are fixed. A piece of double-sided pressure sensitive adhesive (PSA) cut into the shape of a microfluidic channel is fitted around the fixed sample. A coverslip is placed on top of the adhesive above the imaging region and two hydrophobic polydimethyl siloxane (PDMS) end caps are attached to the ends of the channel. These are used to maintain the spherical radius of the droplets for more efficient passive pumping.

Inside the microfluidic system, antibodies are presented to the cells that are fixed to the slide (Figure 1B). Using the PLASMIC system allows for extremely small fluid volumes (< 5  $\mu$ l) which in turn reduces reagent consumption without loss of imaging quality. Antibodies targeting 3 antigens are presented in each cycle and then quenched with a tetrazine-black hole quencher (Tz-BHQ) conjugate to remove signal and allow subsequent cycles to be performed.

### Modeling identifies an ideal structure

Different PLASMIC designs were modeled using COMSOL Multiphysics<sup>TM</sup> computational fluid dynamics software to explore the effects of chamber shape on microfluidic mixing during passive flow. A key determinant was fluid velocity within the channel to ensure i) rapid mixing, ii) complete fluid/reagent exchanges and iii) the velocity was low enough to prevent high shear stress (> 0.1 Pa)<sup>17</sup> on the slide surface and which could lead to cellular loss.

Initially, four different channel designs were modeled (Figure 2A). The first design (a circular center well with long entrance channels) had a high velocity, which allowed for rapid fluid exchange, but poor wall mixing in the central region. This design would leave residual antibody and quenching solutions within the system which would have affected

imaging in later cycles. The second design sought to expand the circle into a rounded polygon structure, which improved mixing on the walls, but had a velocity that was out of the range desired for the system. The third design used a larger rectangular channel with rapid expansion and contraction at the entrance and exit respectively. While this reduced the overall velocity and improved mixing, the rapid expansion did not provide sufficient velocity continuity through the channel and the flow could be reduced, requiring more fluid. Therefore, a fourth design was tested with a longer entrance and exit region and a smaller central area. While the mixing was slightly decreased in this design, the velocity remained high enough to ensure that fluid would be exchanged at a rapid rate in the system.

With the channel design selected, effects of increasing channel width (to improve mixing and increase the analysis area) were tested (Figure 2B). As expected, the increased width improved the overall mixing, but too large of an increase reduced the fluid velocity at the wall to nearly zero. For the final design then, a width of 4.5 mm was used to ensure sufficient area to analyze cells while also providing a sufficient flow rate to reduce excess reagent use.

### Microfluidic device assembly and testing

The selected channel design was designed to be 10 mm long by 4.5 mm wide (Figure 3A). This channel was cut out of double-sided adhesive tape and then adhered to a glass slide. To complete assembly of the device, a glass coverslip was attached over the center region of the channel and two PDMS pieces with 1.5 mm access ports were attached to each end of the channel (Figure 3B). The size of the device allows for up to 4 individual systems to be imaged on a single slide (standard width, 75 mm), which increases the multiplexing capability of the system.

To ensure optimal signal when imaging, double-sided adhesives of varying thickness (50  $\mu\text{m}$ , 100  $\mu\text{m}$ , 130  $\mu\text{m}$ , and 150  $\mu\text{m}$ ) were tested to determine the maximum fluorescence signal of polystyrene bead standards. Beads of similar size as cells ( $D = 10 \mu\text{m}$ ) were imaged and then compared to a control of beads sandwiched between a slide and a coverslip. By analyzing the signal-to-noise ratio (SNR) of beads from each system, it was determined that a thickness of 50  $\mu\text{m}$  resulted in the highest SNR at a value of  $\sim 2.4$  (Figure 3C) with increasing thickness resulting in a significant drop in SNR (150  $\mu\text{m}$  SNR =  $\sim 1.5$ ). Figure 3D compares the traditional method of simply placing a glass coverslip over the sample and the PLAMIC system by the cell loss percentage and the additional cost after each image cycle. With traditional methods 0.5–2.5% of cells was lost each cycle on average, and a similar level of cell loss was observed with the PLAMIC system. The additional cost of each cycle was significantly reduced ( $> 20\%$  less than traditional) with the device due to marked decrease in the volume of antibody cocktail required to stain the cells.

To demonstrate efficient quenching, the signal to background ratio (S/B) of the labeled and quenched cycles were plotted (Fig. 3E) for splenocyte cycling. The S/B of the antibody labeling was measured in the 647 nm channel and averaged for 5 separate experiments. The markers imaged in each cycle were CD4 (cycle 1), CD11c (cycle 2), and Ly6C (cycle 3). The S/B was high ( $> 2$ ) indicating good signal differentiation from background and improved

with later cycles. The S/B during the quench cycles was consistent as the experiment progressed, demonstrating efficient loss of signal upon quenching.

### The device enables repeat cyclic imaging of mouse immune cell markers

Freshly harvested mouse splenocytes were used as a model system to benchmark the device for cyclic imaging (Figure 4) along with a panel of standard immune cell markers. We utilized FAST imaging, which exploits highly accelerated bioorthogonal tetrazine/*trans*-cyclooctene (Tz/TCO) click reaction to enable iteration of rapid quenching and re-staining of immunofluorescence as described in our previous studies<sup>3, 4</sup>. FAST probes were synthesized with a ternary scaffold containing a fluorophore (AF488, AF555, or AF647), a TCO for clicking with a Tz-labeled quencher (Black hole quencher, BHQ3), and a NHS/TFP-ester for reaction with amine-containing molecules such as antibody. Cells were stained with antibodies conjugated to the FAST probes and the FAST fluorophores were quenched using Tz-BHQ3 in between cycles. A total of four cycles, containing 3 markers each, were performed on cells fixed in the microfluidic device. The results of this experiment showed robust labeling in each cycle with minimal overlap in signal from prior cycles. Furthermore, it was easy to image the exact same region of the slide for each cycle since the device was fixed in place. Minimal cell loss was observed as the cycling progressed (< 10%, Figure 3D).

### MC38 tumor immune profiling

To show applicability of the device for tumor immune cell profiling, we imaged 8 immune markers (CD45, CD8, CD4, CD11b, F4/80, MHCII, CD11c, Ly6C) in cells directly harvested by FNA of MC38 mouse colon cancer, an immunogenic tumor model. The choice of the tumor model and immune cell markers was based on our previous studies on tumor-infiltrating immune cell populations<sup>4, 18</sup>. Cells were attached to the surface of a glass slide using Cytospin, and the device was layered on top of the cells prior to imaging.

Profiling of these tumor samples revealed a diverse immune profile (Figure 5) within the tumor FNA. Both myeloid and lymphoid cells were observed to be present, with signal from the labeled cells well above the background (~2 SNR/cycle). This experiment consisted of 4 cycles, each containing two markers and demonstrated efficient quenching of the signal between cycles. Similar to the splenocyte sample, imaging of the same region was easily possible due to the slide being fixed in place on the stage over the course of the experiment. Cell loss was again minor (< 10%), which is promising for prolonged use of this system with heterogeneous samples.

## Discussion

In this work, we describe a microfluidic device for the cyclic imaging of cellular biomarkers in single-cell suspension samples such as those obtained by FNA biopsy. FNA samples are commonly obtained during cancer and other disease work-ups and processed by chromogenic staining for cytopathology<sup>19</sup>. Cyclic imaging, i.e., repeat staining and destaining of scant cellular specimen, allows much deeper biomarker analysis based on diverse immune and cancer markers<sup>3, 20, 21</sup>. Manual handling of such samples, however,

is cumbersome and labor-intensive, a reason for which we explored microfluidic systems. An overarching goal of this work is to develop inexpensive designs that could be readily employed in LMIC and other resource-limited settings.

The PLASMIC device developed here was simple to manufacture with a cheap desktop craft cutting system. The device allowed for reduced reagent consumption and improved imaging reliability during different staining cycles. Flow in the microfluidic device was generated using passive pumping. Passive pumping relies on varying surface tension within different sized droplets, which is known as Young-Laplace equation and is given as:

$$\Delta P = \frac{2\gamma}{R_i} \quad (1)$$

where  $P$  is the pressure within the droplet,  $\gamma$  is the surface tension of the fluid and  $R_i$  is the radius of the droplet. As a droplet becomes larger, the internal pressure decreases creating a low pressure point. The smaller the droplet, the higher the internal pressure and fluid would be driven towards the low pressure point in the system, which in this case would be the larger diameter droplet. This is a constantly stable system due to the increasing size of the sink droplet and decreasing size of the source droplet, thus allowing flow to always occur (until the fluid is depleted at the source). This principle also ensures reduced backflow in the system, which could potentially contaminate the sample with quencher or antibody from previous cycles.

Traditionally, cell samples are imaged on a glass slide with a coverslip on top. To manipulate the cells after and during imaging, this coverslip must be removed which could potentially cause a significant loss of cells from shear. Furthermore, removing the slide from the imaging system introduces potential error to find the exact same fields of view for cyclic imaging. However, layer-stack microfluidics would provide a stable system that allow to manipulate cells while preventing cell loss. Layer-stack microfluidics have been used for applications such as tangential flow filtration, hemodialysis and cell culture<sup>17, 22–24</sup>. These systems all involve imaging as a method of analysis, though they are often limited in the ability to do so at high resolution. In order to accomplish high resolution imaging in layer-stack devices, they must often be disassembled, which could lead to cell loss, similar to the slide and coverslip method of imaging. Our system circumvents these limitations by its inherent simplicity: a single layer with a coverslip for imaging affords high resolution microscopy while maintaining the small volumes that are beneficial in microfluidic applications.

To determine the optimal channel thickness we explored different tape thicknesses. In an ideal scenario, the channel should be as deep as possible to accommodate cells but as narrow as possible to avoid refractive index mismatches between the air objective and imaging through buffer above the cell/bead sample. Typically, cancer cells adherent to glass have thickness of about 5–20  $\mu\text{m}$ , not accounting for occasional cell clusters. To obtain comparable results across different experimental set-ups, we used 8  $\mu\text{m}$  fluorescent polystyrene beads to mimic cells inside chambers of different thicknesses. Figure 3C shows that the S/B of the beads was highest with the 50  $\mu\text{m}$  channel and decreased for deeper

channels. We attribute this to an ideal optical light path, avoiding unnecessary refractive index mismatches or the need to use water/oil immersion objectives.

The PLASMIC system was tested by imaging two different populations of cells: mouse splenocytes and MC38 colon adenocarcinoma fine needle aspirates obtained from tumors implanted into mice. Aspirated cells were briefly fixed and then spread onto poly-L-lysine coated microscopic slides to which the PLASMIC system was attached. This protocol demonstrated high repeatability and efficiency across a range of experiments. High cell density was observed in both splenocytes and tumor FNA samples. Specifically, it was possible to clearly identify and differentiate cells derived from both the myeloid lineage (Ly6G+ neutrophils, F4/80+ macrophages, etc.) and the lymphoid lineage (CD4/CD8+ T cells) in both the splenocyte (Figure 4) and tumor (Figure 5) samples.

The PLASMIC system is not limited to cyclic immune profiling and can be applied to other scenarios including cyclic imaging of extracellular vesicles with low applied shear, low volume cell culture with *in situ* imaging capabilities, and tissue section imaging with fiducial markers for improved registration during cyclic imaging. The advantage of constraining a system with the PLASMIC layers is that reagent volume will always be significantly reduced without loss of labeling efficiency. Thus, passively pumped, layer-stack microfluidics have the potential to reduce experimental costs significantly, providing an advantage in LMIC applications. In addition, we are exploring the use of the PLASMIC system for cyclic, multiplexed RNA fluorescence *in situ* hybridization (FISH). By reducing the volume of FISH reagents used, the cost of the experiment is reduced. Furthermore, the low volume constraints of the system would allow for faster diffusion of the FISH probes in solution to the target, potentially reducing the required labeling time and speeding up the lengthy FISH process massively. We envision that the use of PLASMIC systems for these variety of applications will improve access to life-saving diagnostics in both standard and LMIC clinical settings.

## Conclusion

We describe a novel method for rapid, inexpensive cyclic imaging for point of care settings. We termed this method passive pumping layer stack microfluidics (PLASMIC), in which the system consists of a simple layer of pressure sensitive adhesive designed in the shape of a channel. Fluid was exchanged in this channel using passive pumping, which allowed for small volumes to minimize reagent costs and shear-induced cell loss. Using the PLASMIC system, we demonstrate cyclic imaging of immune and tumor cells in typical fine needle aspirate samples often obtained clinically. Future work will study the functionality of the system for alternative analysis techniques (FISH, IHC) and samples (extracellular vesicles, tissue sections).

## Materials and Methods

### Layer-stack microfluidic device design and production

We explored a number of adhesive tapes, differing in adhesive (acrylic, silicone), polymer thickness (50  $\mu\text{m}$  - 300  $\mu\text{m}$ ) and color (clear, semi-transparent, black). A large number of

such tapes have been developed in the past for other industries including automotive and aerospace applications as well as the electronics industry. For our application, we required uniform thickness, inertness and non-leachability of interfering substances during repeat stain and wash cycles. Zero autofluorescence and good performance in wet conditions were also important features. The tapes tested included 3M Very High Bond (VHB) and standard double-sided adhesives, double-sided optical tape, and ultrathin (300  $\mu\text{m}$ ) silicone sheet material (3M). We ultimately settled on 50  $\mu\text{m}$  thick 3M VHB tape (F9460PC) due to the increased signal observed while imaging and the stability and lack of leaching over the course of several days.

Layer-stack microfluidic device patterns were prepared using Affinity Designer. These designs were exported as scalable vector graphics (SVG) files to Inkscape and then converted to drawing interchange format (DXF) files for import into the craft cutter software.

Channels were cut from the 50  $\mu\text{m}$  thick, double-sided adhesive tape using a Silhouette Cameo 4 craft cutting tool (Silhouette USA). The files were imported into the Silhouette software and re-scaled to the appropriate dimensions. The blade settings for the cut were as follows: Speed = 1; Thickness = 33; Blade Setting = 7; Line Segment Overcut = On, 0.2 mm. Cut tape layers were adhered to the glass slides around the spot of fixed cells applied via a Cytospin centrifuge (Thermo Scientific). The device was completed with the addition of a glass coverslip (No. 1.5) and two PDMS caps with 1.5 mm holes as inlet and outlet ports.

### Computational fluid dynamics modeling

Device designs were modeled using COMSOL Multiphysics™ Computational Fluid Dynamics modeling software (COMSOL v5.3). Devices were designed within the software and modeled using the fluid flow physics package for steady state flow. A 2D model of the fluid path was generated, the fluid was set to water, and pressure boundary conditions were added to the inlet and outlet of the system. Fluid pressures were calculated using the Young-Laplace equation (Equation 1) and set as input and output pressures accordingly. Assuming radii of 1 mm and 3 mm for the two droplets and surface tension of 72 mN/m for a droplet of water, then the force in each droplet is expected to be 144 Pa for the 1 mm droplet and 48 Pa for the 3 mm droplet with a pressure drop of 96 PA across the channel. The other boundaries were modeled as no-slip walls. Devices were modeled to scale to ensure accurate representation of the system. The mesh size was kept at the default value (normal). A time dependent study over the course of 60 seconds was performed and fluid velocities were extracted as streamlines with coloring representative of the fluid velocity along the line.

### Immunostaining and quenching for FAST imaging

Immunostaining within the PLASMIC device was performed as in typical immunofluorescence protocols. The device was first filled with PBS by pipetting fluid through the PDMS port on one end of the device. After the channel was completely filled, a 5  $\mu\text{L}$  droplet was formed on the exit port while a 1  $\mu\text{L}$  droplet was formed on the inlet port.



All solutions were added 1  $\mu$ L at a time to the inlet port droplet. Total fluid volumes added were 10  $\mu$ L to ensure that the fluid was completely exchanged even though the total system volume was 2.5  $\mu$ L.

Five to ten thousand cells in 20  $\mu$ L of PBS were loaded to an Shandon Octospot well strip (Thermo Scientific) to spin down the cells to a poly-L-lysine coated glass slide by Cytospin (Thermo Scientific, RRID:SCR\_020507). As a result, the cells were attached to a defined area on the glass slide to be contained in a PLASMIC device. Cells were blocked with Intercept buffer (LI-COR Biosciences) for 30 minutes before immunostaining. Antibodies were diluted to 1–5  $\mu$ g/mL in Intercept buffer and cells were incubated with FAST-conjugated antibody cocktail for 30 minutes at room temperature protected from light. Stained cells were washed with PBS before imaging on an Olympus BX63 epifluorescence microscope with a 20x objective (Olympus) equipped with a mercury light source. Using the Olympus MetaMorph software, images were captured at 4 different wavelengths (305 nm, 488 nm, 555 nm, and 647 nm) using filter cubes for DAPI, FITC, Cy3, and Cy5 respectively with exposure times of 100 ms for the 305 nm channel and 300 ms for the remaining three channels.

Following image acquisition, cells were briefly incubated with 10  $\mu$ M Tz-BHQ3 in PBS-bicarbonate buffer (pH 9) for quenching. Residual Tz-BHQ3 was removed by PBS wash, and the cells were imaged again in the same fields of view to record quenched signal. Before the next immunostaining of the subsequent cycle, cells were briefly incubated in a solution of 50  $\mu$ M dTCO-PEG6-CO<sub>2</sub>H in order to block any residual Tz-BHQ3 from reacting with FAST antibodies of the next cycle. The same staining, imaging, and quenching cycle was repeated until all of the target proteins were imaged.

### Synthesis of fluorochrome/quencher pair

FAST probes are designed to include a modular linker between fluorochromes and antibodies with an TCO molecule for clicking with a tetrazine-quencher. FAST probes were synthesized as described in detail in our previous study<sup>3</sup>, stored as the carboxylic acids, and activated for antibody labeling with our *in situ* NHS/TFP activation chemistry. The dTCO-PEG<sub>6</sub>-CO<sub>2</sub>H blocking reagent was synthesized from dTCO-PNP and amino-dPEG<sub>6</sub>-CO<sub>2</sub>H and characterized by LC-MS. All reagents were obtained from commercial sources: Fluorophores were purchased from Click Chemistry Tools or Fluoroprobes; BHQ@-3 Amine from LGC Biosearch Technologies; N- $\alpha$ -Boc-N- $\epsilon$ -Fmoc-Lysine from Chem-Impex; Amino-dPEG@<sub>n</sub>-carboxylic acids (n=4,6) from Quanta BioDesign; Dry solvents and coupling reagents from Sigma Aldrich. rTCO-PNP and dTCO-PNP were a generous gift of Dr. Hannes Mikula (TU Wien, Austria).

### Antibody modifications

Antibodies were purchased as carrier-free for modification with FAST probes as previously described<sup>3</sup>. Antibodies were exchanged into bicarbonate buffer (pH 8.4) using a 40k Zeba column (Thermo Fisher) and incubated with a 5- to 10-fold molar excess of the FAST probe with 10% DMSO for 25 minutes at room temperature in dark. After conjugation reaction, unbound FAST probes were removed by another 40k Zeba column equilibrated with PBS.

To determine the degree of labeling (DOL), the absorbance spectrum of the FAST-labeled antibody was measured using a Nanodrop 1000 (Thermo Scientific). The known extinction coefficients of the dye, IgG antibody, and correction factor of the dye absorbance at 280 nm were applied for calculation of DOL. FAST-labeled antibodies were stored in the dark at 4°C in PBS until use.

## Animals

Wildtype C57BL6 mice (Cat# 000664) with 8 weeks of age were purchased from Jackson Laboratory and implanted with H2B-GFP MC38 tumors. All animals were housed under specific pathogen free conditions at the Massachusetts General Hospital. Experiments were approved by the MGH Institutional Animal Care and Use Committee (IACUC) and were performed in accordance with MGH IACUC regulations.

## Cells

The MC38 cell line was initially a kind gift from Mark Smyth, QIMR Berghofer Medical Research Institute) and has been used by our group previously<sup>25, 26</sup>. Cells were cultured in IDMD media(Thermo Fisher, Cat. # 12440046) supplemented with 10% fetal bovine serum (Thermo Fisher, Cat. # A3840001) and 1% penicillin/streptomycin (Thermo Fisher, Cat. # 15070063). Cells were harvested at ~80% confluency for subcutaneous injection into the flanks of female and male C57BL/6 mice (Jackson Laboratories) (n= 5). For mouse splenocytes, spleens were harvested from C57BL/6 mice right after euthanasia (n=3). Spleens were cut into ~1 mm pieces by clean surgical scissors in RPMI 1640 media (Thermo Fisher, Cat. # 11875101) and ground against a 70 µm cell strainer using the back end of a 10 mL syringe plunger. The cell strainer was washed with 10 mL RPMI1640 media to collect cells from homogenized tissue. Collected cells were incubated in ACK lysis buffer (Lonza, Cat. # 10–548E) for 3 minutes on ice for blood cell removal and washed in PBS. Isolated splenocytes were fixed immediately in 4% paraformaldehyde for 10 minutes, washed in PBS, and stored in Intercept buffer (Li-cor Biosciences, Cat. # 927–70001).

## Mouse tumor fine needle aspirate (FNA)

MC38 cells expressing H2B-GFP were obtained by transducing MC38 cells with LentiBrite Histone H2B-GFP Lentiviral Biosensor (Merck, Cat#17–10229, titer  $1.75 \times 10^9$  IFU/mL). Transduction was performed with a multiplicity of infection of 20 for 24 hours. GFP+ cells were sorted using a FACSAria I (BD Biosciences) cell-sorting system after 10 days of culture. For tumor implant, C57BL6 mice (Jackson Laboratory) were injected subcutaneously with  $2 \times 10^6$  of the H2B-GFP MC38 cells in 50 µL of sterile PBS. When tumors reached 40 mm<sup>3</sup> in size after 1–2 weeks of tumor cell injection, mice were anesthetized with 2% isoflurane inhalation for the FNA procedure. An FNA sample was obtained by inserting and withdrawing a 25G needle several times within the tumor tissue, applying slight negative pressure in the syringe attached to the needle. Collected cells were flushed out of the needle with 200 µL PBS into an Eppendorf tube. FNA samples were immediately fixed in 4% paraformaldehyde (PFA) and attached to poly-L-lysine coated glass slides using a Cytospin centrifuge (Thermo Scientific, RRID:SCR\_020507) at 850 rpm for 5 minutes prior to imaging. Octospot 8-well strips (Thermo Scientific) was used to attach cells in a defined area on glass slides.

## Supplementary Material

Refer to Web version on PubMed Central for supplementary material.

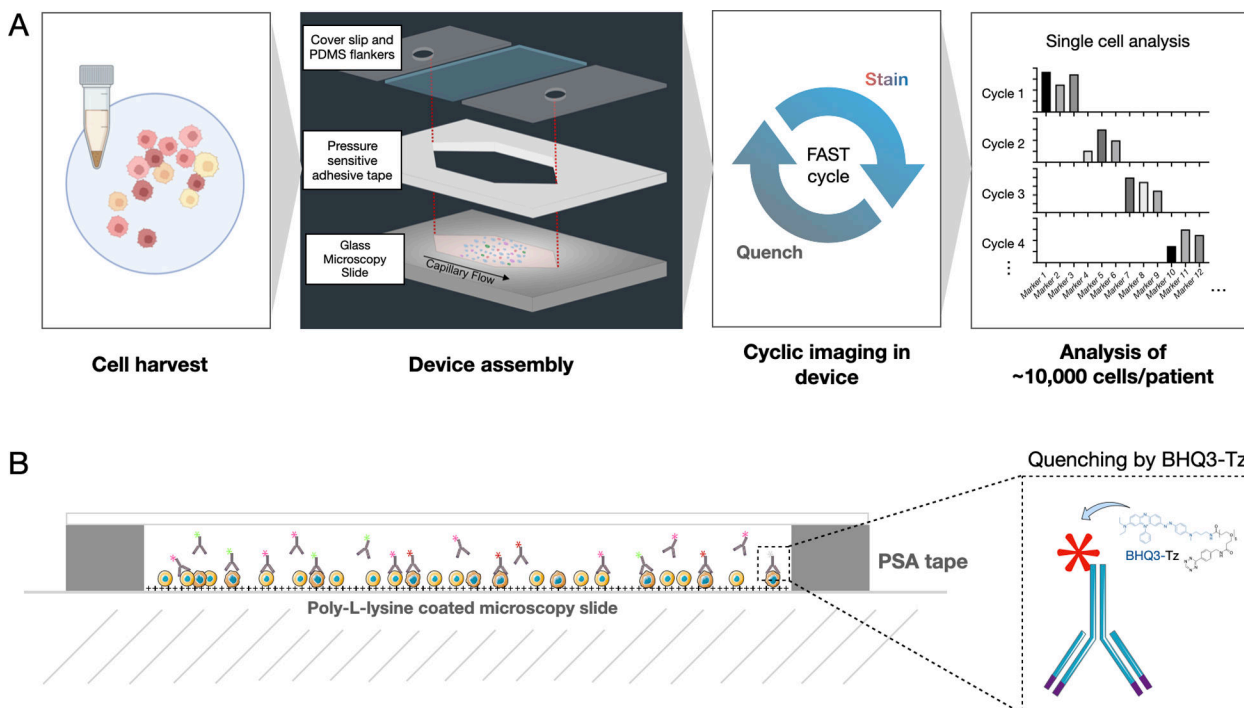
## Acknowledgments

We acknowledge the help and many discussions with our colleagues at CSB including Drs. Jonathan Carlson, Claudio Vinegoni, Hyungsoon Im and Hakho Lee. We also acknowledge the help of Joshua Spitzberg and Jaehee Kim in the early phases of the research. Cartoons in Figure 1A were created on [BioRender.com](https://www.biorender.com). The following funding sources were used to support certain aspects of the work: R01CA257623, R21CA236561 and CSB development fund. KL was supported by T32-CA079443.

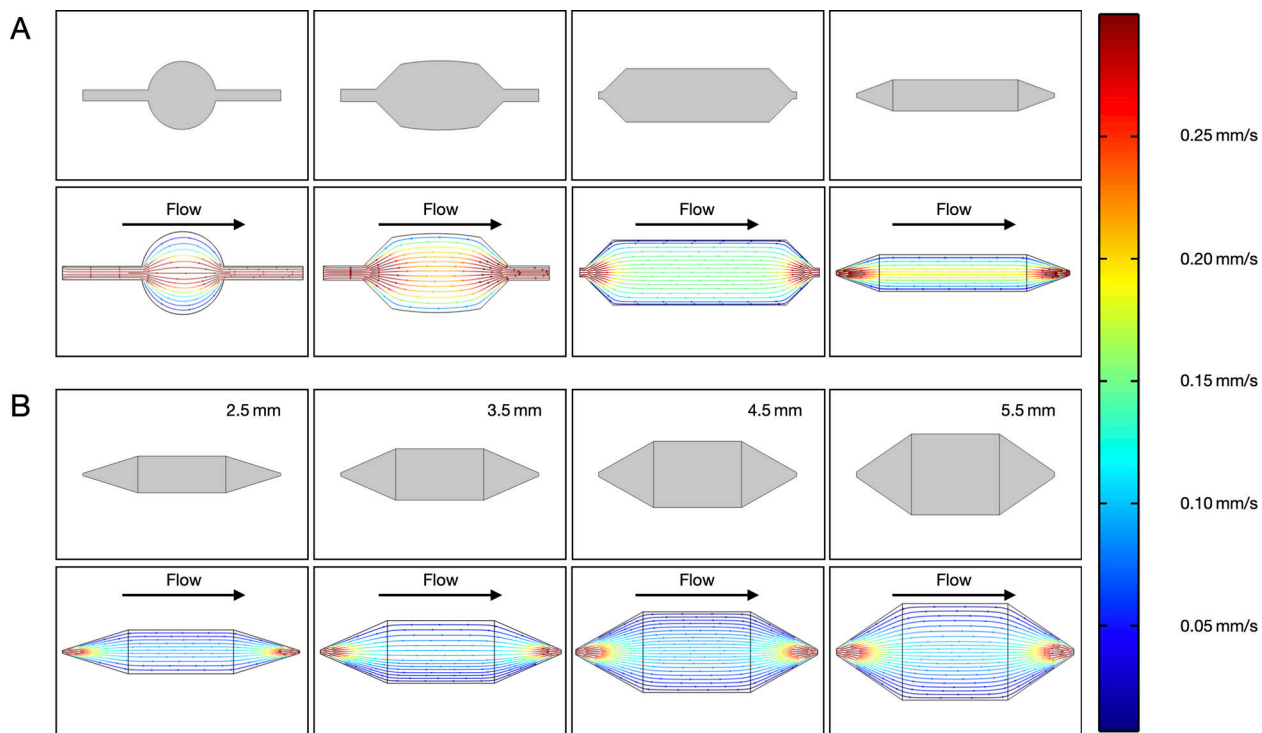
## References:

1. Boyd JD, Smith GD, Hong H, Mageau R and Juskevicius R, *Cytometry Part B: Clinical Cytometry*, 2015, 88, 64–68. [PubMed: 25196066]
2. Frenk NE, Spring L, Muzikansky A, Vadvala HV, Gurski JM Jr, Henderson LE, Mino-Kenudson M, Ly A, Bardia A and Finkelstein D, *JCO Precision Oncology*, 2017, 1, 1–9.
3. Ko J, Oh J, Ahmed MS, Carlson JC and Weissleder R, *Angewandte Chemie*, 2020, 132, 6906–6913. [PubMed: 34366494]
4. Oh J, Carlson JC, Landeros C, Lee H, Ferguson S, Faquin WC, Clark JR, Pittet MJ, Pai SI and Weissleder R, *Clinical Cancer Research*, 2021, 27, 4781–4793. [PubMed: 34233961]
5. Min J, Chin LK, Oh J, Landeros C, Vinegoni C, Lee J, Lee SJ, Park JY, Liu A-Q and Castro CM, *Science Translational Medicine*, 2020, 12.
6. Weissleder R and Lee H, *Nature Reviews Materials*, 2020, 5, 409–422.
7. Shinde P, Mohan L, Kumar A, Dey K, Maddi A, Patananan AN, Tseng F-G, Chang H-Y, Nagai M and Santra TS, *International journal of molecular sciences*, 2018, 19, 3143.
8. Narayanamurthy V, Jeroish Z, Bhuvaneshwari K, Bayat P, Premkumar R, Samsuri F and Yusoff MM, *RSC Advances*, 2020, 10, 11652–11680. [PubMed: 35496619]
9. Teh S-Y, Lin R, Hung L-H and Lee AP, *Lab on a Chip*, 2008, 8, 198–220. [PubMed: 18231657]
10. Zheng S, Lin HK, Lu B, Williams A, Datar R, Cote RJ and Tai Y-C, *Biomed Microdevices*, 2011, 13, 203–213. [PubMed: 20978853]
11. Streets AM, Zhang X, Cao C, Pang Y, Wu X, Xiong L, Yang L, Fu Y, Zhao L, Tang F and Huang Y, *Proc Natl Acad Sci U S A*, 2014, 111, 7048–7053. [PubMed: 24782542]
12. Cheng YH, Chen YC, Lin R, Brien S, Jung YT, Chen W, Lee Z, Hao S, Sahoo H, Min Kang J, Cong M, Burness S, Nagraath SWM and Yoon E, *Nat Commun*, 2019, 10, 2163. [PubMed: 31092822]
13. Liu Y, Yang M, Deng Y, Su G, Enniful A, Guo CC, Tebaldi T, Zhang D, Kim D, Bai Z, Norris E, Pan A, Li J, Xiao Y, Halene S and Fan R, *Cell*, 2020, 183, 1665–1681.e1618. [PubMed: 33188776]
14. Zhou J, Wu Z, Hu J, Yang D, Chen X, Wang Q, Liu J, Dou M, Peng W, Wu Y, Wang W, Xie C, Wang M, Song Y, Zeng H and Bai C, *Science Advances*, 2020, 6, eabc1204. [PubMed: 33219024]
15. Nguyen H-T, Thach H, Roy E, Huynh K and Perrault CM-T, *Micromachines*, 2018, 9, 461.
16. Thuo MM, Martinez RV, Lan W-J, Liu X, Barber J, Atkinson MB, Bandarage D, Bloch J-F and Whitesides GM, *Chemistry of Materials*, 2014, 26, 4230–4237.
17. Mossu A, Rosito M, Khire T, Li Chung H, Nishihara H, Gruber I, Luke E, Dehouck L, Sallusto F, Gosselet F, McGrath JL and Engelhardt B, *J Cereb Blood Flow Metab*, 2018, DOI: 10.1177/0271678X18820584, 271678X18820584.
18. Garris CS, Arlauckas SP, Kohler RH, Trefny MP, Garren S, Piot C, Engblom C, Pfirschke C, Siwicki M and Gungabeesoon J, *Immunity*, 2018, 49, 1148–1161. e1147. [PubMed: 30552023]
19. Roskell DE and Buley ID, *Journal*, 2004, 329, 244–245.
20. Lin J-R, Fallahi-Sichani M and Sorger PK, *Nature communications*, 2015, 6, 1–7.

21. Goltsev Y, Samusik N, Kennedy-Darling J, Bhate S, Hale M, Vazquez G, Black S and Nolan GP, *Cell*, 2018, 174, 968–981. e915. [PubMed: 30078711]
22. Johnson DG, Khire TS, Lyubarskaya YL, Smith KJ, Desormeaux JP, Taylor JG, Gaborski TR, Shestopalov AA, Striemer CC and McGrath JL, *Adv Chronic Kidney Dis*, 2013, 20, 508–515. [PubMed: 24206603]
23. Dehghani M, Lucas K, Flax J, McGrath J and Gaborski T, *Advanced materials technologies*, 2019, 4, 1900539. [PubMed: 32395607]
24. Lucas K, Dehghani M, Khire T, Gaborski T, Flax JD, Waugh RE and McGrath JL, *Journal of Membrane Science*, 2021, 633, 119357.
25. Oh J, Magnuson A, Benoist C, Pittet MJ and Weissleder R, *JCI insight*, 2018, 3.
26. Rodell CB, Ahmed MS, Garris CS, Pittet MJ and Weissleder R, *Theranostics*, 2019, 9, 8426. [PubMed: 31879528]

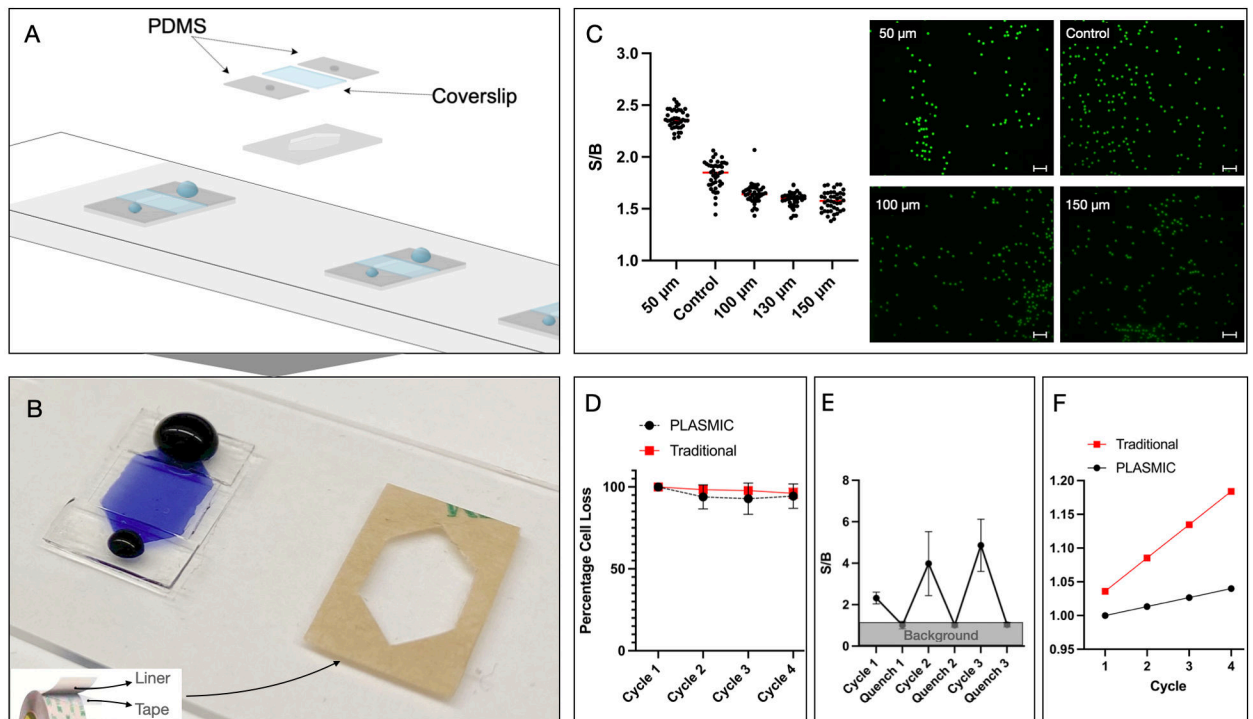


**Figure 1: Cyclic imaging in passively pumped, layer-stack microfluidic (PLASMIC) devices.**  
**A)** Harvested cells are attached to the glass slide and the PLASMIC system is directly placed on top of the cells. Once covered with a cover slip and PDMS flankers, cyclic FAST imaging can be performed in the device. The immune profile of approximately 10,000 cells/FNA can be extracted and analyzed for tumor specific data at the single cell level.  
**B)** The FAST probes used in this study contain an antibody-fluorochrome complex with a TCO-containing linker that clicks with a BHQ3-Tz moiety, and enables quenching of the fluorescent signal after each imaging cycle. Repeat staining and quenching allows for multiplexed single-cell analysis.



**Figure 2: Computational fluid dynamics simulations of device designs.**

**A)** Different channel shapes were tested to determine the best design based on mixing and fluid velocity. It was determined that a long expansion from the fluid entrance into a wide, straight channel provided the best combination of sufficient velocity and mixing for this method. **B)** With the shape selected, the effects of channel width were further studied. It was determined that a channel width of 4.5 mm maintained efficient mixing while also having a high enough velocity to reduce reagent consumption.



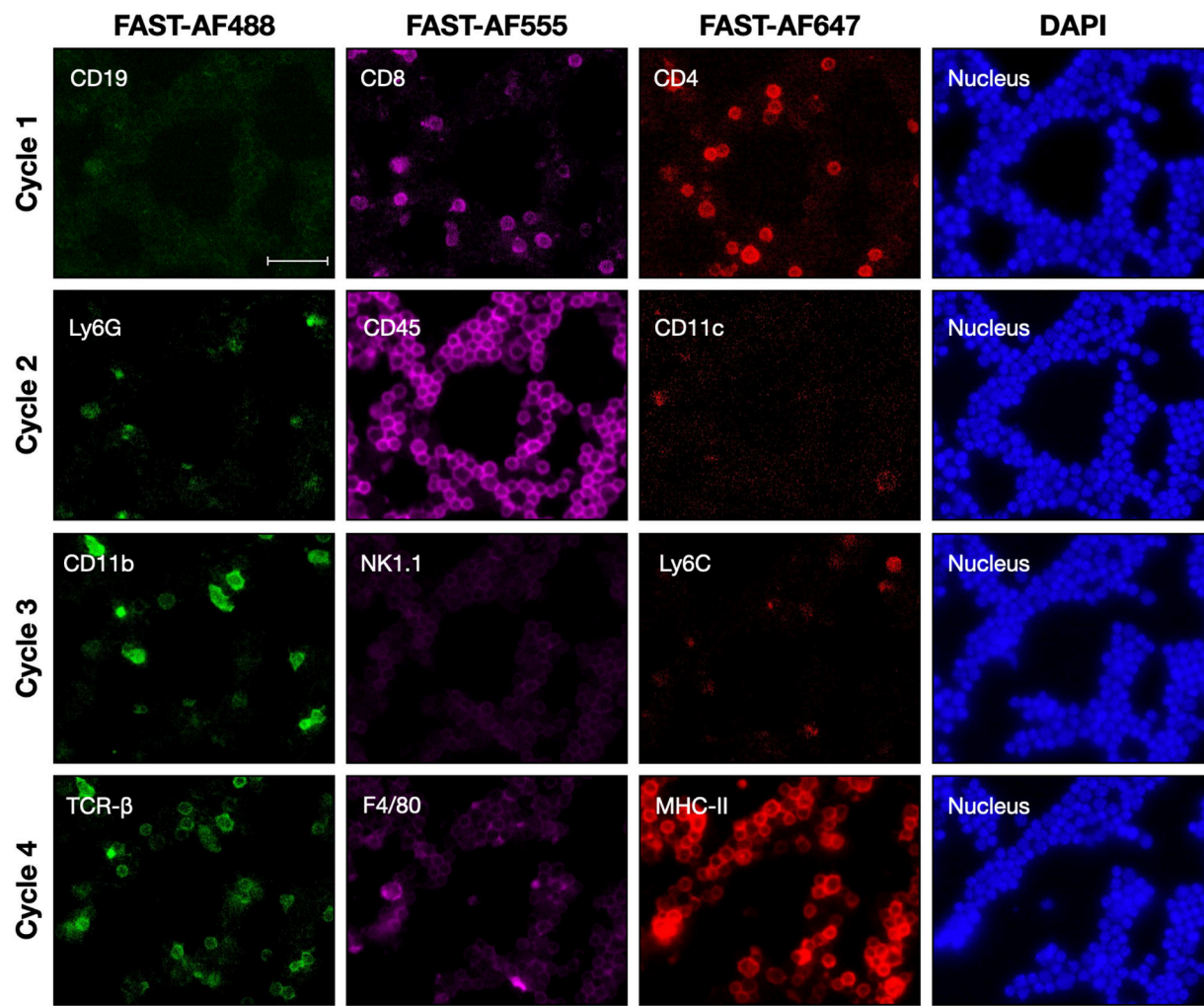


**Figure 4: Cyclic imaging of murine splenic immune cells.**

Imaging in the PLASMIC showed robust labeling of the cells throughout four cycles, shown here in each of the four rows. Cells were obtained as primary isolates from spleens of normal C57/B6 mice. These splenocytes contain a number of different immune cells of lymphoid and myeloid lineage. The cells were labeled with different fluorescently labeled antibodies against immune cell surface markers. Nuclei were stained with DAPI to provide a reference between individual staining cycles. Quenching with the FAST Tz-BHQ/TCO chemistry proved to be rapid (< 5 min) and efficient with minimal label from previous cycles. Nuclear staining showed minimal cell loss from shear (< 10%) demonstrating the efficiency and sensitivity of the passive pumping technique. Scale bar = 10  $\mu$ m.



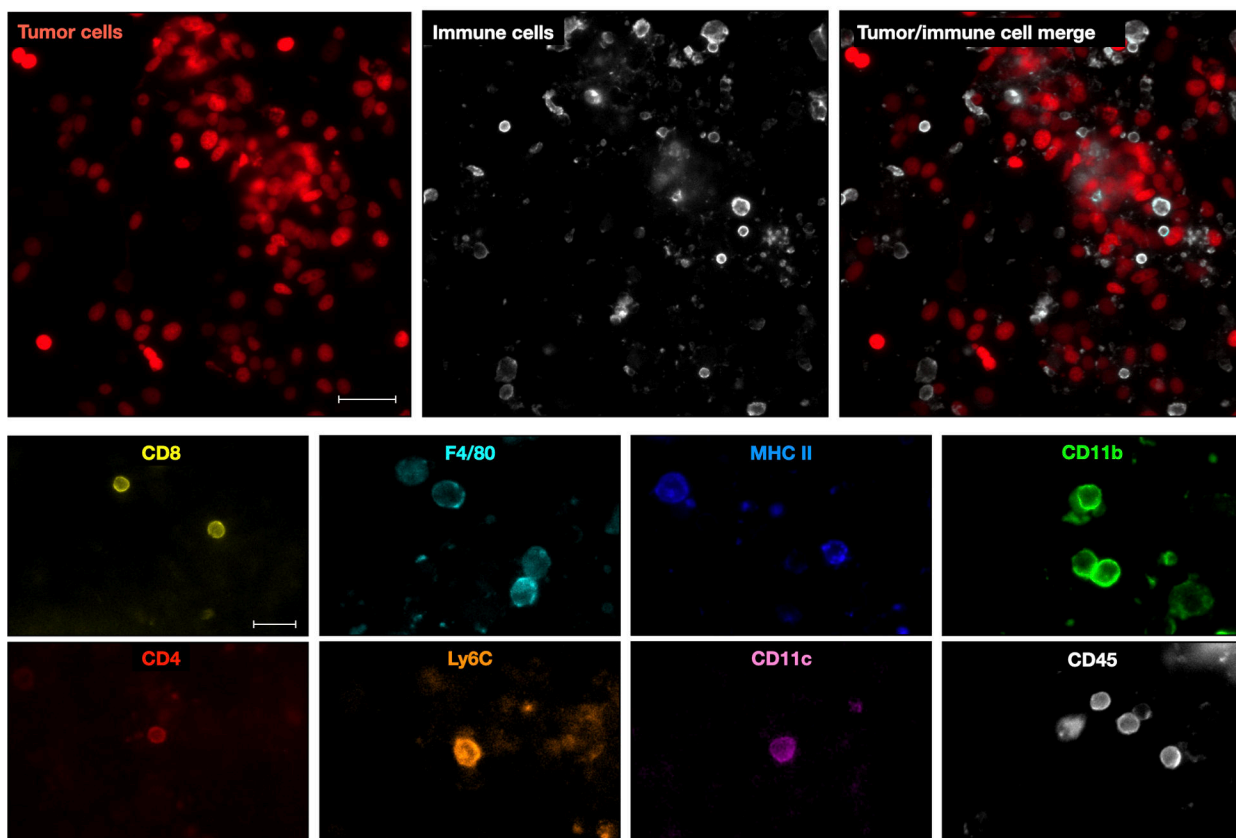


**Figure 5: Tumor cell profiling.**

Fine needles aspirates were obtained from MC38 colorectal tumor bearing, immunocompetent C57/B6 mice. The cells were stained for 8 different immune cell markers in 4 consecutive cycles to analyze immune infiltration into the tumor micro environment. CD45 labeling (white) shows multiple immune cells present in the FNA sample, distinct from the GFP labeled MC38 colorectal tumor cells (red, top row). The immune cell population is diverse and cells of multiple phenotypes can be observed in the sample as indicated in the lower half. Scale in first row = 100  $\mu$ m. Scale in second row = 20  $\mu$ m.